Available online at www.sciencedirect.com
SCIENCE DIRECT®
Nuclear Instruments and Methods in Physics Research A 499 (2003) 549–559
NUCLEAR INSTRUMENTS & METHODS IN PHYSICS RESEARCH Section A
www.elsevier.com/locate/nima

PHENIX inner detectors

M. Allen[a], M.J. Bennett[b], M. Bobrek[c], J.B. Boissevain[b], S. Boose[d], E. Bosze[e], C. Britton[c], J. Chang[e], C.Y. Chi[f], M. Chiu[f], R. Conway[b], R. Cunningham[b], A. Denisov[g], A. Deshpande[h], M.S. Emery[c], A. Enokizono[i], N. Ericson[c], B. Fox[h], S.-Y. Fung[e], P. Giannotti[d], T. Hachiya[i], A.G. Hansen[b], K. Homma[i], B.V. Jacak[b], D. Jaffe[c], J.H. Kang[j], J. Kapustinsky[b], S.Y. Kim[j], Y.G. Kim[j], T. Kohama[i], P.J. Kroon[d], W. Lenz[d], N. Longbotham[k], M. Musrock[c], T. Nakamura[i], H. Ohnishi[d], S.S. Ryu[j], A. Sakaguchi[i], R. Seto[e], T. Shiina[l], M. Simpson[c], J. Simon-Gillo[b], W.E. Sondheim[b], T. Sugitate[i], J.P. Sullivan[b,*], H.W. van Hecke[b], J.W. Walker[c], S.N. White[d], P. Willis[k], N. Xu[a]

[a] *University of Tennessee, Knoxville, TN 37996, USA*
[b] *Los Alamos National Laboratory, Los Alamos, CA 87545, USA*
[c] *Oak Ridge National Lab, Oak Ridge, TN 37831, USA*
[d] *Brookhaven National Laboratory, Upton, NY 11973-5000, USA*
[e] *University of California, Riverside, CA 92521, USA*
[f] *Columbia University, New York, NY 10027 and Nevis Laboratories, Irvington, NY 10533, USA*
[g] *Institute for High Energy Physics (IHEP), Protvino, Russia*
[h] *RIKEN BNL Research Center, Brookhaven National Laboratory, Upton, NY 11973-5000, USA*
[i] *Hiroshima University, Kagamiyama, Higashi-Hiroshima 739-8526, Japan*
[j] *Yonsei University, Seoul 120-749, South Korea*
[k] *Abilene Christian University, Abilene, TX 79699, USA*
[l] *University of Alabama, Huntsville, AL 35899, USA*

The PHENIX Collaboration

Abstract

The timing, location and particle multiplicity of a PHENIX collision are determined by the Beam–Beam Counters (BBC), the Multiplicity/Vertex Detector (MVD) and the Zero-Degree Calorimeters (ZDC). The BBCs provide both the time of interaction and position of a collision from the flight time of prompt particles. The MVD provides a measure of event particle multiplicity, collision vertex position and fluctuations in charged particle distributions. The ZDCs provide information on the most grazing collisions. A Normalization Trigger Counter (NTC) is used to obtain absolute cross-section measurements for p–p collisions. The BBC, MVD and NTC are described below.

PACS: 25.75.−q; 29.40.Ka; 29.40.Mc; 29.40.Gx

Keywords: Relativistic heavy-ion collisions; Cherenkov detectors; Scintillation detectors; Tracking and position sensitive detectors

*Corresponding author. Tel.: +1-505-665-5963; fax: +1-505-665-7920.
E-mail address: sullivan@lanl.gov (J.P. Sullivan).

0168-9002/03/$ - see front matter © 2002 Published by Elsevier Science B.V.
doi:10.1016/S0168-9002(02)01956-3

1. Introduction

The PHENIX detector [1] at the Relativistic Heavy Ion Collider (RHIC) is designed to perform a broad study of A–A, p–A and p–p collisions to investigate nuclear matter under extreme conditions. The characteristics of the interactions of projectiles at the PHENIX interaction diamond are determined by the Beam–Beam Counters (BBCs) and the Multiplicity/Vertex Detector (MVD). The BBCs [2] are composed of two arrays of Cherenkov counters with quartz radiators and photomultiplier readout each located just outside the poles of the central magnet. The BBC provides both the time of interaction and its position from the flight time of prompt particles. The time of interaction is used as a start time for the time-of-flight (ToF) measurement and a signal for the Level-1 (LVL1) trigger to limit the vertex region within the PHENIX acceptance. Typical BBC results from the first year of PHENIX running are described. The MVD provides a measure of event multiplicity, collision vertex position and fluctuations in charged particle distributions. It consists of Si strip detectors in concentric barrels around the beam pipe and endcaps of Si pad detectors. The NTC is used to enhance beam normalization measurements during polarized proton running. The ZDC [3] is described elsewhere in this volume.

2. Beam–beam counters

The main role for PHENIX BBC is to provide the time of beam–beam collisions for the ToF [4] measurement, to produce a signal for the PHENIX LVL1 trigger and to measure the collision vertex point (ZVTX) along the beam axis. Since the longitudinal size of the beam bunch at RHIC for Au–Au collisions is designed to be 25 cm RMS, the time spread of nuclear collisions could be as much as 2 ns. Charged hadron identification by the ToF system requires its resolution to be less than 100 ps for the whole ToF system, thus allowing pion–kaon separation up to 2.4 GeV/c with a 4σ standard deviation. The precise measurement of the ToF start time determined by the BBC is critical for the identification of hadrons.

2.1. BBC requirements and detector configuration

The BBC consists of two identical sets of counters installed on both sides of the collision point along the beam axis, one on the North side and the other on the South side of the PHENIX interaction region where each counter is named BBCN and BBCS, respectively. The BBCs are placed 144 cm from the center of the interaction diamond and surround the beam pipe. This corresponds to a pseudorapidity range from 3.0 to 3.9 over the full azimuth.

The BBC needs to satisfy the following requirements:

(i) The number of charged particles generated by Au–Au collisions at $\sqrt{s_{\mathrm{NN}}} = 200$ GeV within the BBC acceptance is as much as a few thousands for central collisions. Moreover the BBC also needs to operate with p–p collisions up to $\sqrt{s} = 500$ GeV. The BBC must thus have a capability to function over a large dynamic range from 1 MIP to 30 MIPs.

(ii) Since the BBC is placed in a very high-level radiation area around the beam pipe near the interaction point, it is required to be radiation hard.

(iii) The BBC is installed just behind the PHENIX central spectrometer magnet. The expected magnetic field along the beam axis around this location is 3 kG. Therefore the BBC needs to work in a high magnetic field environment.

After studying the possibilities carefully, we chose the following configuration to satisfy the above requirements. Each counter is composed of 64 1-inch diameter mesh-dynode photomultiplier tubes (Hamamatsu R6178) equipped with 3 cm quartz on the head of the PMT as a Cherenkov radiator. Fig. 1(a) and (b) show individual BBC elements and the BBC array mounted on the BBC mechanical frame, respectively. The outer diameter of the BBC is 30 cm and the inner diameter is 10 cm with clearance between the beam pipe and the BBC of 1 cm. For this configuration the expected number of charged particles for a central

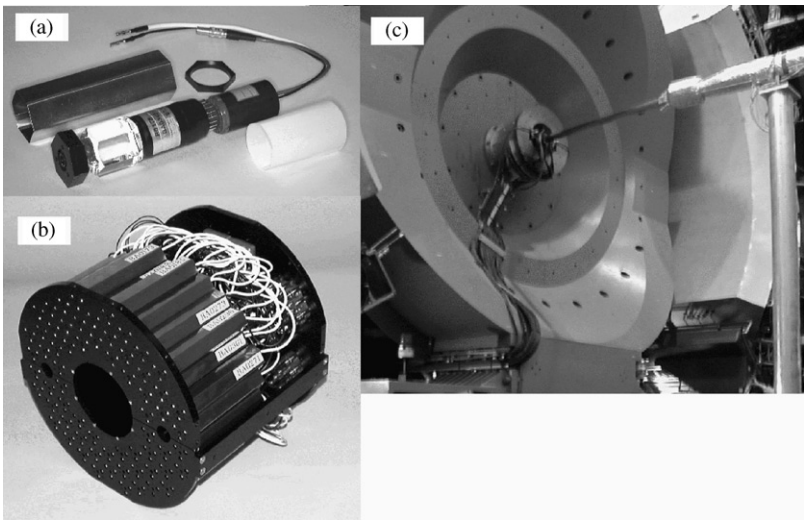

Fig. 1. (a) Single BBC consisting of 1 in mesh dynode photomultiplier tubes mounted on a 3 cm quartz radiator; (b) A BBC array comprising 64 BBC elements; and (c) The BBC is shown mounted on the PHENIX detector. The beam pipe is seen in the middle of the picture. The BBC is installed on the mounting structure just behind the central spectrometer magnet.

Au–Au collision at $\sqrt{s_{NN}} = 200$ GeV is expected to be 15 particles per BBC element. A laser signal which is used by the ToF and ElectroMagnetic Calorimeter (EMCal) [5] calibration systems is also delivered to individual BBC elements to monitor and calibrate the drift of the timing for the ToF measurement. The BBC system has eight high voltage channels for each side. A single high voltage supply operates at least eight BBC elements. To equalize the PMT gains the BBC elements are divided into 16 groups of tubes with similar gain based on cosmic-ray measurements. Operational high voltage is set to obtain 75 pC output charge for a MIP particle from each BBC element.

The temperature inside the BBC is a problem for BBC operation since 64 PMTs are confined to a very small space. With no cooling the temperature can exceed 75°C which may cause electric shorts of the cable inside the bleeder circuit. To avoid this problem an air flow of 200 l/min is used to cool the BBC. Moreover, 32 thermocouples are installed inside the BBC to monitor the temperature. Flow meters are also installed to measured the air flow rate. The information from the thermocouples and flow meters is connected to the BBC high voltage interlock system so that if the temperature inside the BBC exceeds 50°C, or no air flow is detected in the BBC cooling system, the high voltage system for the BBC is shutdown immediately by the interlock system. Fig. 1(c) shows the BBC installed in the mounting fixture on the central spectrometer magnet. Fig. 2 in the PHENIX Overview article [1] gives a view of the BBC in relation to the rest of the PHENIX detector.

2.2. BBC readout electronics and PMT gain adjustment

The BBC readout electronics chain consists of discriminators, shaping amplifiers, time-to-voltage converters (TVC) and flash ADCs (FADC). The time and pulse height information is digitized in real time and is stored in digital buffer memories. The BBC provides the LVL1 trigger with an input signal thus the timing and pulse height of BBC elements are digitized during each beam crossing by the TVC and FADC and stored at the same time in the buffer memory. A detailed description of the front-end electronics used in the PHENIX detector is found elsewhere in this volume [6].

The gains of the PMTs were adjusted using the MIP peak in the pulse height distribution. Fig. 2 shows a typical pulse height distribution for a BBC

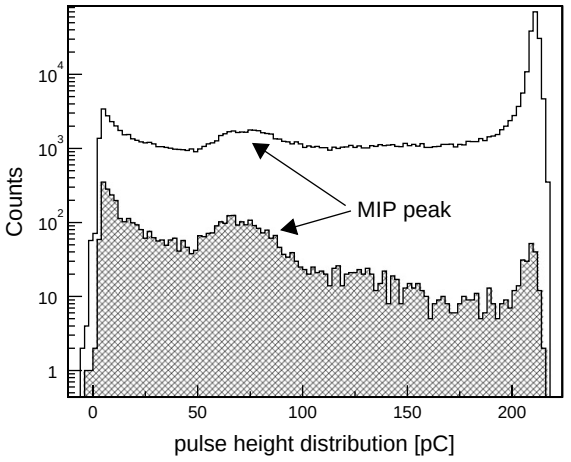

Fig. 2. Typical pulse height distribution for a BBC element. The hatched area shows the same distribution for low-multiplicity events where less than 10 valid hits on the 64 BBC elements are required. The peak at the high pulse height end is due to overflow.

element. The hatched area in this figure shows the same distribution for low multiplicity events where less than 10 valid hits out of 64 BBC elements are required. The MIP peaks are visible at approximately 75 pC on the x-axis. The variation of the PMT gains was 20% RMS.

2.3. Calibration and time resolution

Each BBC measures arrival times of leading charged particles from beam collisions. The arrival time for each BBC (T_S and T_N) is defined as the average of the hit time in each BBC. The systematic shift of timing of individual BBC elements from the average hit time is mostly caused by the time walk by the discriminator and time offset in individual BBC elements. The following empirical formula was used for the time walk and time offset correction to get a precise time:

$$T_{\mathrm{corr}} = T_{\mathrm{raw}} - T_{\mathrm{offset}} - C/\sqrt{Q} \quad (1)$$

here, T_{raw} is the uncorrected arrival time, T_{offset} is the time offset in each individual BBC element, Q is the charge of the signal as measured with the FADC and C is the coefficient of the time walk. T_{offset} and C are determined by minimizing the residual time $\delta t_i = T_{\mathrm{S\ or\ N}} - t_i$ for all BBC elements. The search for the calibration parameters is performed iteratively and the parameters converge within three iterations.

After application of the time calibration to all BBC elements, the time deviation from the average hit time is mostly caused by the time resolution of the particular BBC element, since the average hit times for the north and south BBC arrays are statistically well determined. Fig. 3(a) shows the distribution of timing deviations from the BBC average time for a typical BBC element. The standard deviation of this distribution is defined as the time resolution of each BBC element. Fig. 3(b) shows the distribution of time resolution over all BBC elements. The time resolution of a single BBC element is 52 ± 4 ps (rms) under real experimental conditions. Fig. 4 shows the ToF distribution where the start time is defined by the BBC. The ToF resolution is 96 ps which allows the separation of pions and kaons up to particle momenta of 2.4 GeV/c. The detailed description for the ToF detector is found elsewhere in this volume [4].

2.4. Z Vertex measurement and performance with LVL1 trigger

Fig. 5(a) shows a correlation of ZVTX calculated by BBC and ZDC, and Fig. 5(b) shows the projection of Fig. 5(a) on to the axis of BBC ZVTX. The peak at ZVTX $= \pm 144$ cm in Fig. 5(b) corresponds to beam collisions outside of the BBC.

The ZVTX position and number of hit PMTs in each BBC are also calculated online and sent to the LVL1 trigger. $|ZVTX| < 20$ cm (from the online calculation) and two or more PMTs fired in each BBC are required as the LVL1 trigger condition. The hatched area in Fig. 5(b) corresponds to the events selected by the LVL1 trigger. The trigger efficiency with respect to inelastic Au–Au collisions is evaluated by a PHENIX detector simulation with the HIJING [12] event generator to produce Au–Au collisions as input, and was found to be $92 \pm 2\%$.

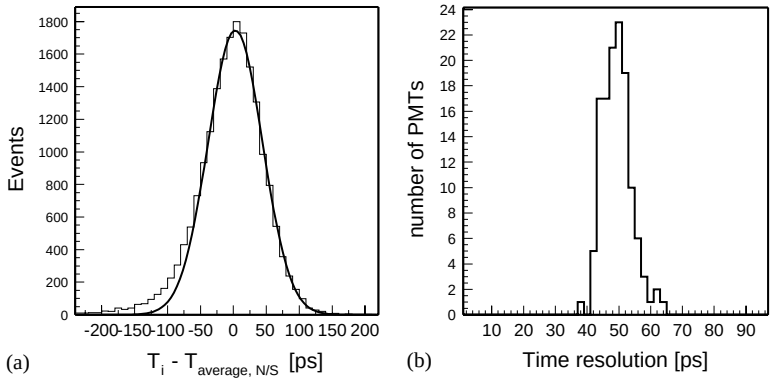

Fig. 3. (a) Distribution of timing deviation for a typical BBC element from BBC averaged hit timing and (b) profile of timing resolution for each BBC element.

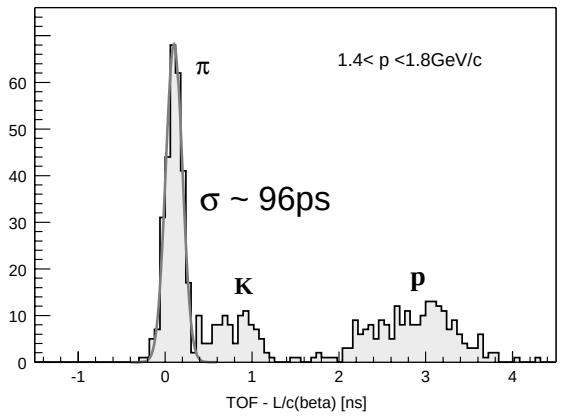

Fig. 4. ToF distribution measured between the BBC and ToF detectors. The start time of the ToF measurement is provided by the BBC and the ToF detector defines the stop time. The ToF in ns is given on the horizontal axis. The ToF is determined by assuming the pion mass for each particle. A detailed description of the ToF measurement is given in Ref. [4].

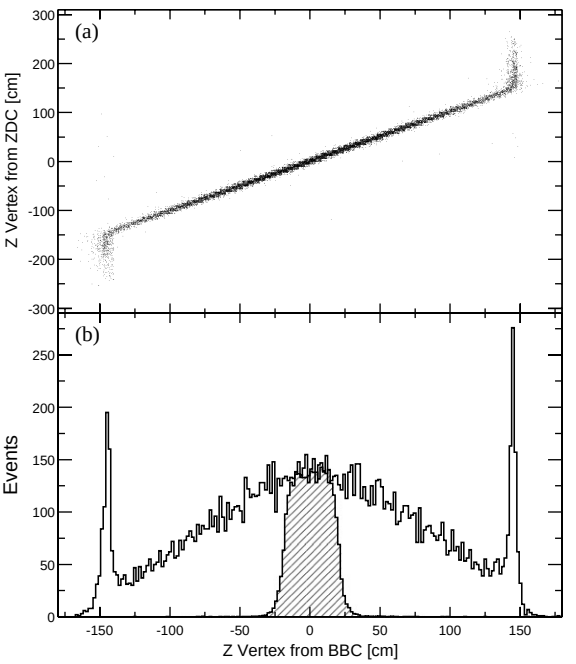

Fig. 5. (a) Correlation of determined ZVTX between BBC and ZDC and (b) ZVTX distribution from BBC. Hatched area corresponds to the events satisfying the PHENIX Local LVL1 trigger condition.

2.5. Centrality measurement

The BBC charge sum has a monotonic correlation with collision centrality. In the offline analysis, the combined information on spectator neutrons measured by the ZDC placed 18 m from the beam crossing point and the charged sum information measured by the BBC is used to define the collision centrality. The correlation between the BBC and ZDC measurements is shown in Fig. 6. The lines shown in Fig. 6 bin the events with centrality beginning on the far right with the 0–5% bin and going to the left at intervals of 5% up to 50%.

2.6. Performance

The BBC is fully implemented and installed in the PHENIX detector complex. The performance

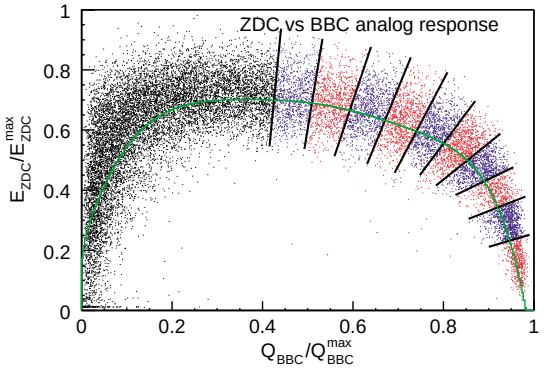

Fig. 6. Correlation between BBC charge sum and energy deposit in ZDC. The lines define bins containing intervals covering 5% centrality. The bin to the far right represents events ranging from 0% to 5% centrality. The central line shown in the figure is the centroid of the BBC–ZDC distribution with the lines defining the centrality bins drawn perpendicular to it.

of the BBC was evaluated using $\sqrt{s_{NN}} = 130$ GeV Au–Au collisions and the arrival time of secondary particles generated by beam interactions, which travel nearly at the speed of light. The collision time (T0) is defined from the average arrival time for the two BBC counters. The timing difference between each counter provides the ZVTX along the beam axis.

All the detector elements and readout electronic channels worked well during the first year of RHIC operation. The timing achieved for a single element was 52 ± 4 ps. The BBC is used as a start counter for the ToF measurement and a ToF resolution of 96 ps was obtained. The collision vertex determined by the BBC is used not only for offline analysis but also for the LVL1 trigger to limit the vertex position. Combined information from the BBC and ZDC is used to define the collision centrality in the offline analysis.

3. Multiplicity vertex detector

The PHENIX Multiplicity Vertex Detector (MVD) provides event characterization and selection, measures fluctuations in charged particle production and provides a collision vertex position. The design criteria included large rapidity and good azimuthal coverage and granularity while also minimizing costs and material in the electron arm acceptance. A discussion of the simulation of the performance of the MVD has been published [7].

3.1. Design of MVD

The MVD consists of two concentric barrels of silicon strip detectors (300 μm thick and 200 μm pitch) around the beampipe and two disk-shaped endcaps of silicon pad detectors at $z \approx \pm 35$ cm, where z refers to the beam axis. The length of the active part of the silicon strip barrels is approximately 64 cm. The basic mechanical element of the barrels is the "C-cage". A sketch of a C-cage is shown in Fig. 7.

A C-cage is made of light-weight rigid rohacell foam (density 0.075 gm/cm^3) with Si detectors glued to the inner and outer surfaces. Flexible kapton cables, with 50 μm thick copper traces, carry the signals from the detectors to Multi-Chip Modules (MCMs) which are the first stage of the front-end electronics. The barrel is constructed of 12 of these C-cages stacked end-to-end to form 1/2 of the barrel. The inner barrel consists of the detectors glued to the inner surface of the rohacell. It is 5 cm from the beam line. The outer barrel is 7.5 cm from the beam line. A completed half of the MVD, including some of the other mechanical and electronic parts is shown in Fig. 8. The second half is a mirror image of the first. The two halves are connected by a hinge at the bottom. They "clam-shell" open in order that they lift up and then close around the beam pipe. The inner barrel has 72 positions (6 azimuthal times 12 longitudinal) populated. The outer barrel with $R = 7.5$ cm will be only partially populated with Si to reduce the amount of material in the electron arm acceptance. The top 2/3 of the detector will omit the detectors in the eight C-cages nearest the center of the MVD.

A few of the pad detectors can be seen in Fig. 8. Most are hidden from view by the barrel but parts of several wedges can be seen just below the far end of Fig. 8 and to the left of the barrel. Each endcap of the MVD contains 12 wedge-shaped pad

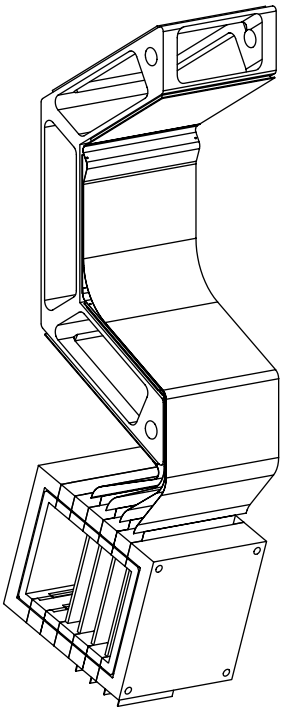

Fig. 7. A diagram of an MVD "C-cage". Si detectors are glued to a rohacell foam cage. Kapton cables connect the Si to MCMs which are enclosed in a cooling plenum, also made of rohacell.

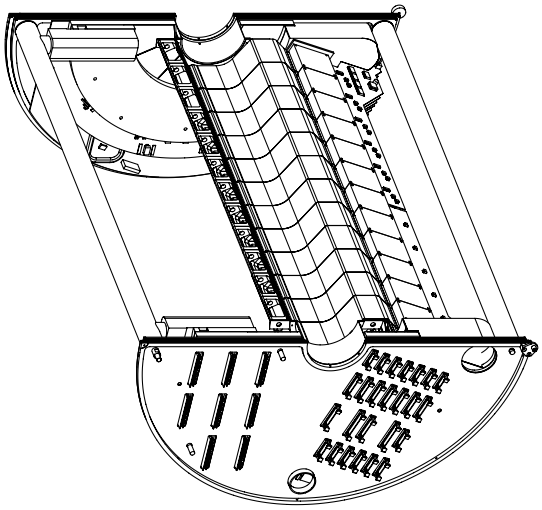

Fig. 8. A diagram of one half of the MVD barrel. Some of the mechanical support structure has been removed from the diagram to make the interior visible.

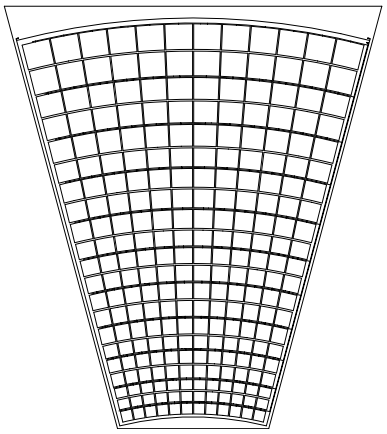

Fig. 9. A diagram of a MVD pad detector. The trapezodial-shaped readout pads are shown.

detectors. Each pad detector is divided into 12 azimuthal (ϕ) segments and 21 radial segments. The radial segments increase from 2.5 to 5 mm going from the innermost radial position (5 cm) to the outermost (12 cm). This is done to keep the pseudorapidity (dη) coverage of each pad roughly constant. A diagram of one of the pad detectors is shown in Fig. 9.

The single-event coverage about midrapidity is five units in η for the inner barrel layer and four units in η for the outer barrel layer. The η coverage for event-averaged quantities is extended due to the variation of the vertex position along the direction of the colliding beams. The disk-shaped endcaps cover $1.79<|\eta|<2.64$ for an event at $z=0$. The vertex position can be located using hits in the barrel for z positions between -40 and -40 cm, which covers the majority of the length of the interaction region ($\sigma=22$ cm).

3.2. MVD readout

Both the MVD pad and strip detectors are read out with identical MCMs, which are optimized for minimum size and power dissipation. The MCMs [8] are constructed by the High Density Interconnect (HDI) process at Lockheed-Martin Corporation. They are approximately $43\times48\times1.5\ \text{mm}^3$ with a mass of 13.0 g. The substrate is alumina. Each MCM contains eight TGV-32 preamplifier/discriminator chips [9] and eight

analog memory unit plus ADC chips (AMU/ADC) [10]. The TGV-32 and AMU/ADC chips each have 32 channels. In addition, the MCMs contain two Xilinx 4010E Field Programmable Gate Arrays (FPGAs), a temperature sensor (AD590) and an op-amp (CLC426). One of the FPGAs is called the Address List Manager (ALM) and is used to control the read and write addresses to/from the 64-deep AMUs in the AMU/ADC chips. The second FPGA is called the Heap Manager (HM) and is used to control most of the other logic signals on the MCM. After a level-1 accept is received, it collects all 256 ADC values from the MCM, constructs the serial data packet containing the ADC values and then sends it off from the MCM.

A kapton cable connects up to six MCMs in the barrel to a power/communications board. These boards can be seen at the bottom of the barrel in Fig. 8. In the complete MVD, the north and south half each contain 12 power/communications boards. These, in turn, are connected in groups of six to "mother boards". The mother boards are approximately the shape of one half of a disk and are in the endcaps of the MVD. One ring-shaped "daughter board" is also attached to each mother board. The daughter board has 6 MCMs attached to it. Each of these six MCMs is wire-bonded directly to a Si pad detector. In Fig. 8 the Si pad detectors can be seen, but the MCMs and the daughter boards are obscured by a cooling plenum which covers them. The data packets are sent out of the MVD via cables connected to the mother boards. The mother boards are also connected to timing and control cables which bring in the 9.5 and 38 MHz clocks for the MCMs as well as various control signals including the level-1 accept. There are also serial-control cables for each power/communications and daughter board connected to the mother board. These are used to load the Xilinx programs in the MCMs, and to set and read back various serial control bits in the MCMs, the AMU/ADCs and the TGV32s.

The data packets coming off of the mother boards are connected via 7 m shielded ribbon cables to Data Collection Interface Modules (DCIMs) [11] in a rack below the intersection region. One DCIM module is associated with each power/communications board or daughter board. The DCIMs serve as buffers for the data (they can hold up to 7 data packets in FIFOs), slightly modify the data packets and also convert the incoming Low Voltage Differential Signals (LVDS) to a Glink serial output format on a single optical fiber. These fibers go to the PHENIX data acquisition system.

The MCMs and the chips on them were designed to minimize power dissipation. The MCMs associated with the Si strips are contained in a rohacell plenum, which can be seen in Figs. 7 and 8. Each MCM dissipates 1.8 W (about 7 mW per input channel), which is small enough to allow the MCMs to be cooled by chilled air blown through the plenum. The MCMs associated with the pad detectors are in a separate plenum, but are also air cooled. Each mother board contains 38 voltage regulators. The relatively localized heat generated by these regulators is removed by water cooling lines glued to the back of the mother-board. Temperature, air flow and water flow sensors throughout the cooling system are connected to a set of custom circuit boards which automatically shut off power to the affected part of the MVD when a problem arises.

3.3. Low mass construction of MVD

The MVD design minimizes the amount of material "seen" by the electron arms. The purpose is to reduce the background from photon conversion to e^+e^- pairs in the material in the MVD. As part of this effort, most of the mass is concentrated at the endcaps or at the bottom of the MVD. In general, only the lower energy electrons ($\lesssim 200$ MeV/c) produced in the material at the bottom of the MVD (mainly the MCMs and the power/communications boards) are bent into the central arm acceptance by the field of the central magnet. If only the material on a straight line path from the MVD to the central arms is considered, the inner shell represents 0.17% of a radiation length, the rohacell in the C-cages represents an average thickness of 0.074% of a radiation length, the outer shell 0.18% of a radiation length, each kapton cable represents 0.042% of a radiation length and each layer of Si represents 0.32% of a

radiation length. The amount of Si and the number of layers of kapton varies with position in the barrel, but the minimum is 0.42% (no Si, no kapton), the maximum is 1.23% (two Si and four kapton layers) and 0.79% is "typical" (one Si, one kapton).

3.4. MVD performance

The second year of RHIC running will be the first year of data taking for the MVD. As an example of the expected performance Fig. 10 shows a bench-top test of a single Si-strip channel with a ^{106}Ru source. The source passed through a Si-strip detector into a trigger scintillator. The readout was through the MVD readout hardware. The trigger scintillator was large (22×22 mm^2) compared to a single Si strip, so most events are in the "pedestal" of the ADC distribution shown in Fig. 10. However, the few percent of all events which actually hit this single strip are clearly separated from the pedestal. The signal to noise ratio is 14/1. In this example, common mode noise (i.e. noise common to all 256 channels) was removed in the analysis. We expect to be able to do this for the real detector setup also, either by better grounding and shielding (preferable) or in the offline analysis. Before removing the common mode noise the signal to noise was 7.4/1 which was only adequate.

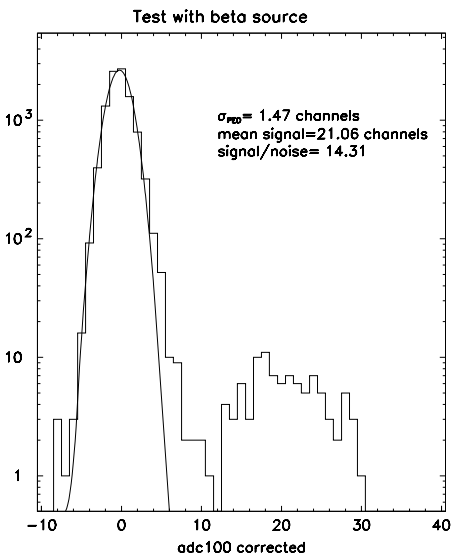

Fig. 10. ADC distribution for a ^{106}Ru β^- source in a single Si-strip channel. The pedestal is much larger than the signal because the trigger scintillator (22×22 mm^2) was much larger than the strip (5×0.02 cm^2) shown in this sample plot.

4. Normalization trigger counters

A Normalization Trigger Counter (NTC) has been installed in the vertex region of the PHENIX detector. This additional counter is necessary to enhance normalization measurements during p–p running using polarized protons. The NTC consists of two identical fiber-readout scintillation counters, each situated between the endplate of the MVD and the brass nosecone in the vertex region on the north and south sides, respectively, of the PHENIX detector.

For p–p collisions where the average multiplicity is much less than for heavy ion collisions a normalization device with a greater coverage of the cross-section than that provided by the BBCs is needed. The latter sees approximately 60% of the cross-section but the addition of the NTCs increases this number to approximately 85%. As a result of this increased coverage, the error in the total p–p cross-section is reduced significantly, thereby improving the ability to use the p-p data to compare with that from heavy ion running. In addition, the knowledge of the relative luminosity of different bunches is critical for the spin program. The NTC aids this effort by providing another measurement to compare with the ZDC and BBC coincidence rates, thereby assuring that this critical quantity is measured correctly.

The NTCs are also helpful in a number of other ways. They provide a means for separating beam gas from beam–beam events by forming a coincidence between the NTC counters on each end of the PHENIX detector. In order to fulfill this requirement the NTC time resolution is in the subnanosecond range. The NTCs also give an efficient and clean trigger with a different bias than the other "standard" PHENIX triggers, thereby aiding in understanding the bias of events collected during p–p running. They can also provide a

means of rejecting the unacceptable rate of cosmic-ray events in the muon arms.

The NTC scintillators are situated in the gap between the MVD and the nosecone and cover the radial area between the beam pipe and the outer ring of the MVD. The fibers from the scintillators run along the surface of the nosecone up to the phototubes. The phototubes, along with the coupling enclosure for the fibers, are placed in an aluminum structure which is affixed to the nosecone.

Fig. 11 is a drawing for a single counter. One is installed on either end of the PHENIX detector. The counter is constructed from four $40 \times 40\ cm^2 \times 5.1$ mm thick pieces of BC-404 (polyvinyltoluene-base) plastic scintillator into which 80 cm long, 1 mm thick Bicron BCF-92-WLS wave-shifting fibers have been embedded in grooves cut into the surface of the scintillator. The fibers are glued into place using BC-600 optical epoxy. The upper quadrants are glued to the lower quadrants to form halves that are light sealed using a wrapping made of a combination of BC-638 Black (0.2 mm thick) Tape, BC-642 PTFE Reflector (0.08 mm thick) Tape and BC-620R TiO_2 Reflector Paint. Each half is encased by 0.25 mm thick stainless steel to protect the fibers and the surface. The thickness of the counter is less than 9.5 mm. Each NTC detector half is attached to the MVD endplate at three points along the outer diameter via aluminum brackets and three points on the inner diameter via set screws attached to an aluminum extension to the inner diameter framework of the MVD.

The unattached ends of fibers from each quadrant of the NTC counter are bundled together and optically coupled to a Hamamatsu H6614-01 phototube operating at a maximum voltage of -2500 V. Each phototube is in a light-tight enclosure in an aluminum tube which is mounted on the brass nosecone. The phototubes are near a He bag and He degrades their performance. Therefore air from the BBC compressed gas system flows through the gap between the phototube enclosure and the outer aluminum tube. The signals from the 8 phototubes are fed into the

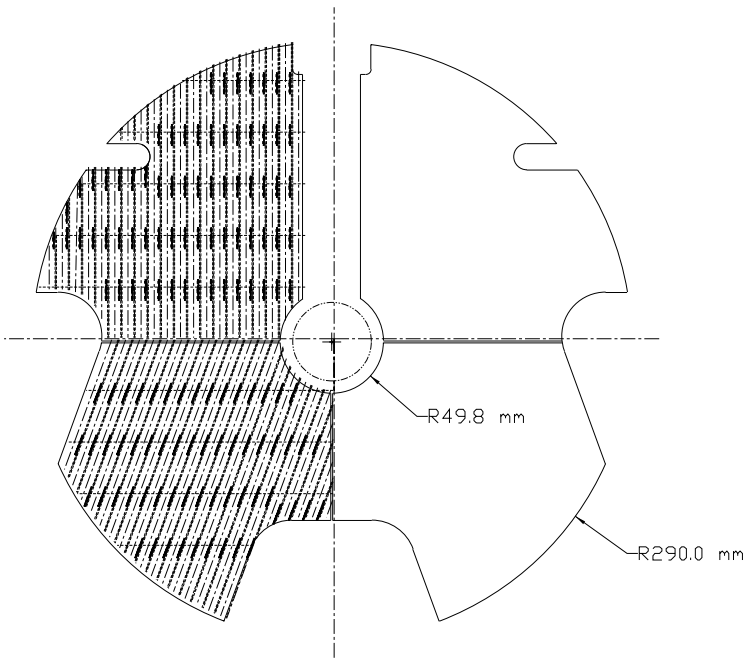

Fig. 11. Schematic diagram of one of the two identical NTC scintillators. In the left half of the figure the pattern of wave-shifting fibers is shown.

PHENIX data-acquisition system via 8 m Belden 8214 cables and the HV is fed to the detectors via Belden RG-59 high-voltage cables.

The NTC was operational for the p–p run during the second year of PHENIX data taking. The efficiency of the NTC will be mapped using electrons from the National Synchrotron Light Source at Brookhaven to determine any non-uniformities. The timing resolution was determined in place in the PHENIX beamline to be about 600 ps using precise timing from the BBCs. This resolution was sufficient to allow inclusion of the NTC in the interaction trigger. The data collected using this interaction trigger was a critical factor in obtaining accurate cross-section measurements during the p–p run.

Acknowledgements

We acknowledge support from the Department of Energy (USA) and MEXT (Japan).

References

[1] K. Adcox, et al., PHENIX detector overview, Nucl. Instr. and Meth. A, (2003) this volume.
[2] K. Ikematsu, et al., Nucl. Instr. and Meth. A 411 (1998) 238.
[3] C. Adler, et al., Nucl. Instr. and Meth. A 470 (2001) 488.
[4] M. Aizawa, et al., PHENIX central arm particle ID detectors, Nucl. Instr. and Meth. A, (2003) this volume.
[5] L. Aphecethe, et al., PHENIX calorimeter, Nucl. Instr. and Meth. A, (2003) this volume.
[6] S.S. Adler, et al., PHENIX on-line systems, Nucl. Instr. and Meth. A, (2003) this volume.
[7] M.J. Bennett, et al., IEEE Trans. Nucl. Sci. NS-46 (1999) 2022.
[8] S.F. Hahn, et al., IEEE Trans. Nucl. Sci. NS-47 (2000) 802.
[9] C.L. Britton, et al., Rev. Sci. Instrum. NS-70 (1999) 1684.
[10] M.S. Emery, et al., IEEE Trans. Nucl. Sci. NS-44 (1997) 374.
[11] M.N. Ericson, et al., IEEE Trans. Nucl. Sci. NS-45 (1998) 833.
[12] X.N. Wang, M. Gyulassy, Phys. Rev. D 44 (1991) 351.